Composites Part B 216 (2021) 108857

Contents lists available at ScienceDirect

Composites Part B

journal homepage: www.elsevier.com/locate/compositesb

Convenient synthesis of one-dimensional a-SEP@LDH via self-assembly towards simultaneously improved fire retardance, mechanical strength and thermal resistance for epoxy resin

Haijun Zhang, Xiaoping Hu *, Yingru Liu, Suhua Zhang, Zhenzhong Wu

State Key Laboratory for Environment-friendly Energy Materials, School of Materials Sciences and Engineering, Southwest University of Science and Technology, Mianyang, 621010, People's Republic of China

ARTICLE INFO

Keywords:
Self-assembly
Epoxy
Fire retardance
Mechanical strength
Thermal resistance

ABSTRACT

It is essential to develop a class of EP composite with improved fire retardance, mechanical strength and thermal resistance performances for some practical applications, such as in aeronautic and automobile fields. Due to the highly tunable structure of layered double hydroxides (LDHs), transition metals Ni^{2+} and Fe^{3+} were selected as the cation components considering their excellent catalytic charring ability. To overcome the easy agglomeration of LDH during polymer process, sepiolite nanofiber (SEP) was used as a carrier for LDH and thus a novel low-cost one-dimensional flame retardant a-SEP@LDH was successfully synthesized via facile self-assembly. With the addition of 2.3 wt% a-SEP@LDH alone, EP composite owns a V-1 rating in UL-94 test, an LOI value of 31.1%, 21% reduction of peak heat release rate and decreased 16.0% total smoke production. Additionally, the total carbon monoxide production has been decreased by 25.3%. Combining the analyses of the char residue and thermogravimetric infrared spectrometry (TG-FTIR) of EP/a-SEP@LDH systems, the flame-retardant mechanism has been drawn as follows: a) physical solidified char residue by sepiolite nanofibers; b) reinforced char residue thanks to the catalytic charring effect of both Ni/Fe alloy catalyst (originated from partially reduced oxide metals) and Brønsted acid sites in sepiolite. Moreover, the tensile strength and glass transition temperature of EP composite have been enhanced simultaneously. In a nutshell, it is an economically effective channel targeting to improve the comprehensive properties of EP through loading Ni–Fe LDH assisted by sepiolite nanofibers.

1. Introduction

Epoxy (EP) has been the most extensively used thermosets in industry since its discovery in 1909 in view of its outstanding physical and chemical merits [1,2]. Unfortunately, polymers composed of hydrogen and carbon elements are of the most typical flammable materials and present immense fire load [3]. For EP, a large heat and a great amount of smoke are released during its combustion [4]. Therefore, developing various flame retardants (FRs) has been used to enhance the fire safety of EP, including organophosphorus compounds [5–7], phosphamide-based intumescent flame retardant [8], P/N/S-containing [9] or P/N-containing [10] FRs. Indeed, those studies have established EP composites with excellent flame retardant property. However, there still exists two drawbacks undesirably. The one is that the mechanical strength and thermal resistance (decreased glass transition temperature, T_g) of EP composites fail to be balanced [11,12]. For high-performance structural products, e.g., in aeronautic and automobile applications, multifunctional epoxy composite with excellent thermal and mechanical properties is required due to its severe environmental conditions, such as wide temperature variations and many kinds of mechanical stresses [13]. The other one is that the phosphate rock as the original material of phosphorus flame retardant is a limited natural resource [14,15]. Therefore, it is urgently essential to develop a class of EP composite with balanced fire retardancy, mechanical strength and thermal resistance by adding economical filler.

Very recently, the use of inorganic fillers such as clays [16] (layered double hydroxides (LDHs) [17,18], halloysite (HNT) [19], vermiculite [20], montmorillonite [21,22] etc.), carbon materials [23] (graphene oxide (GO) [24–27], carbon nanotube (CNT) [28], carbon black [29], fullerene [30,31] etc.) and new nanomaterial MXene [32] seems to be a suitable strategy to modify the flame retardancy of polymer, due to their low loading, high carbon yield and environmental friendliness. Taking

* Corresponding author.
E-mail address: huxiaoping@swust.edu.cn (X. Hu).

https://doi.org/10.1016/j.compositesb.2021.108857
Received 9 January 2021; Received in revised form 11 March 2021; Accepted 28 March 2021
Available online 1 April 2021

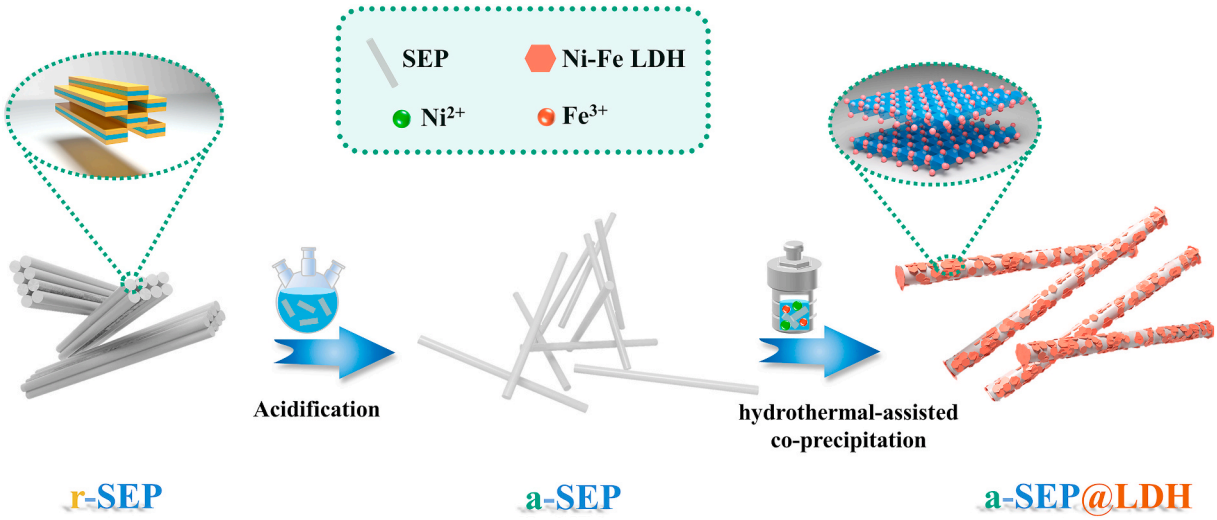

Scheme 1. Preparation route of a-SEP@LDH.

cost-effective and structural flexibility into consideration, LDHs should be an ideal inorganic fillers. LDHs are a class of lamellar compounds with highly tunable structure, reflecting in the species of both cation and intercalated anions [33]. The commonly flame retardant behaviour of LDHs is mainly attributed to the follows a) endothermic decomposition; b) diluting the flammable gases by the evolution of water and some inert gases; c) forming a protectively glassy oxide layer on top of the burning material. Besides, the transition metals in LDHs are capable of catalyzing the pyrolysis products of epoxy into high-quality carbonaceous components [34,35]. Tang et al. have carried on plenty of meaningful work on the investigation of catalyzing carbonization of polymer and proven it is a valid approach to improve the flame retardance of polymers [36]. Transition metals Ni and Fe were reported to synthesize Ni–Fe alloy catalysts for the preparation of carbon nanofibers or carbon nano-onions with high quality [37,38].

However, the major barrier to broaden the application of LDHs is their easily forming stacks after dry during the synthesis of LDHs due to the strong van der Waals interaction between laminates, which has an negative effect on the mechanical and fire-retardant peoteries of polymers [39]. Nowadays, there exists two major strategies to homogeneously disperse LDHs in polymer matrix: a) enlarging the interlayer space of LDHs via different anionic species, such as anionic surfactant (e.g. dodecyl sulfate) [40,41]; b) using support to disperse LDHs, for example, LDH was located on the surface of graphite fiber [42]. Nevertheless, for the former strategy, the synthetic condition of some LDHs systems requires a sealed environment and thus the procedure is of complex. Surprisingly, the latter one shows its merits which can not only combine the characteristics of supports and LDHs but also promote the distribution of LDHs in the polymer matrix. The mechanism for the improved dispersion of LDHs assisted by supporters may be explained by following: the intensive short-range van der Waals attractions among LDH nanosheets themselves are impaired by the long-range electrostatic attractions between supports and LDHs [43].

Sepiolite (SEP), a needle-like natural hydrate magnesium silicate fiber, has a sandwich-like structure composed of two outer sheets of SiO_4 tetrahedra and an inner octahedral sheet of magnesium oxide/hydroxide [44]. Due to its high thermal stability, sepiolite was regularly chosen as a flame retardant synergist to strengthen the residual char on the surface of materials during combustion [45,46]. Furthermore, some interesting natures of sepiolite, including high specific surface area (up to 200–300 m^2/g) [47], more easily dispersible than platelet-like fillers [48], intrinsic mechanical strength (especially in tensile strength [49]) and inexpensive natural resource, make it to be a potential carrier for LDHs.

In the present work, a novel one-dimensional inorganic filler (a-SEP@LDH) composed of SEP and Ni–Fe LDH was designed and synthesized, which stemmed from improving the dispersion of Ni–Fe LDH in EP matric, aiming to enhance the fire safety, mechanical strength and thermal resistance of EP. To the best of our knowledge, no previous effort has been reported about the influence of sepiolite as a carrier for Ni–Fe LDH on the fire safety, mechanical strength and thermal resistance of EP.

2. Experimental section

2.1. Materials

Nickel(II) nitrate hexahydrate [$Ni(NO_3)_2{\cdot}6H_2O$], Iron(III) nitrate nonahydrate [$Fe(NO_3)_3{\cdot}9H_2O$], sodium hydroxide (NaOH) and 4,4-Diaminodiphenyl methane (DDM) were provided by Sinopharm Chemical Reagent Co., Ltd. (Shanghai, China). Ethanol, hydrochloric acid (HCl) and sodium hexametaphosphate (SHMP) were supplied from KeLong Chemical Reagent Co., Ltd (Chengdu, China). Raw sepiolite (SEP) was purchased from Neixiang Dongfeng Sepiolite Limited Liability Company (Neixiang, China). Epoxy resin of diglycidyl ether of bisphenol A (DGEBA, E−44, an epoxy value of 0.43–0.47 mol/100 g) was supplied by Lanxing Resin Co., Ltd. (Lantong, China).

2.2. Synthesis of a-SEP@LDH

Because this sepiolite contains impurities and exists as aggregates bundles, its purification and exfoliation procedures should be carried out before self-assemble. First, the raw sepiolite (r-SEP) was added into deionized water and then undergone vigorous stir and sedimentation procedure. The solid was filtrated and washed by deionized water. Next, the obtained solid was put into deionized water again and stirred 0.5 h with the addition of an appropriate amount of SHMP, subsequently filtered, washed with deionized water and dried. Finally, the pre-treated SEP was dispersed in 5 M HCl aqueous solution and kept stirring around 75–80 °C for 24 h. The products were collected and washed by deionized water until non-existence of chloridion, then vacuum dried at 80 °C for 24 h. The dried residue was powdered and sieved to 200 mesh particle size, abbreviated as a-SEP.

The a-SEP@LDH was synthesized through hydrothermal-assisted co-precipitation method. The a-SEP suspension was prepared firstly: 1.0 g of a-SEP was dispersed in 100 mL of deionized water and ultrasonically stirred for 30 min. Afterwards, the solution containing Ni^{2+} and Fe^{3+} (the mole ratio of Ni^{2+} and Fe^{3+} fixed 3) was dripped into the a-SEP

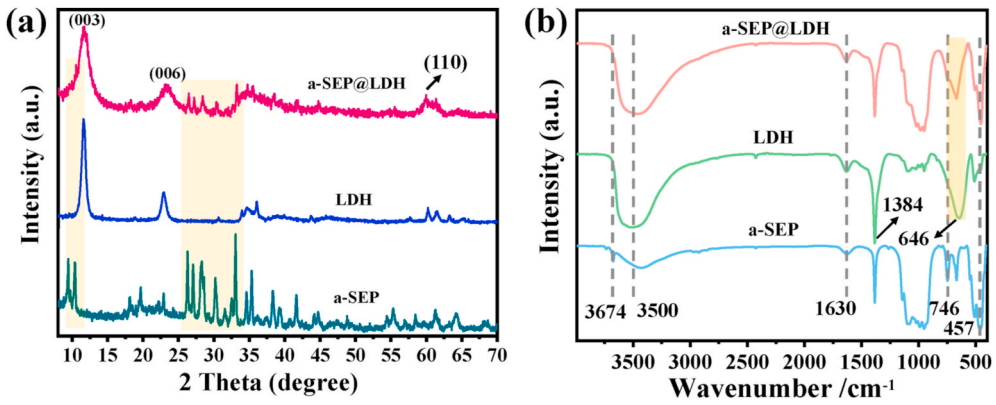

Fig. 1. XRD patterns (a) and FTIR spectra (b) of a-SEP, LDH and a-SEP@LDH.

suspension, and meanwhile, the pH value of the system was maintained around 9–10 by using 3 wt% NaOH aqueous solution. The obtained suspension was continuously mechanical stirred for 4 h at room temperature. Then, the resulting mixture was transferred into a 500 mL Teflon-lined autoclave and heated in an oven at 120 °C for 36 h. After natural cooling to room temperature, the product was collected by filtering and washing with deionized water several times and dried at 70 °C for 24 h. The preparation route is illustrated in Scheme 1. Synthesis of the LDH also utilized the same hydrothermal-assisted co-precipitation method without the addition of a-SEP.

2.3. Preparation of EP and EP composites

The preparation of EP composites containing 2.3 wt% a-SEP@LDH is following: 1.18 g of a-SEP@LDH was added into 50 mL of ethanol and then ultrasonicated to obtain a uniform suspension. Then, the above suspension was fed into the 50 g of the pre-heating EP monomolecular assisted by the mechanical stirring. To get rid of the ethanol, the mixture was heated at 100 °C over 5 h accompanying with constant stirring. Subsequently, 11.2 g of pre-melting DDM was introduced into the mixture, which was then transferred to a vacuum oven to remove bubbles before poured into a preheated polytetrafluoroethylene mold. Finally, the mixture was thermally cured at 120 °C for 3 h and post-cured at 150 °C for 2 h. The preparation procedure of pure EP, EP/LDH, EP/a-SEP and EP/a-SEP-LDH (physical blending, the mass ratio of a-SEP to LDH is 0.8 based on the results of thermogravimetric tests) are the same as the process described above with equal amounts of additives.

2.4. Characterizations

Powder X-ray diffraction (XRD) measurements were conducted on a Japan Rigaku D/Max-1400 rotating anode Xray diffractometer, using Cu Kα radiation (λ = 0.1541 nm) at 40 kV. Fourier transform infrared spectroscopy (FTIR) measurements were carried out using a spectrometer (Perkin-Elmer, USA). Transmission electron microscopy (TEM, Carl Zeiss, Germany) observations were carried on Zeiss Libra 200FE TEM with accelerating voltage 200 kV. Field emission scanning electron microscopy (FE-SEM) was utilized on the MAIA3LMU high-resolution cold field emission scanning microscopy analysis system (TESCAN, The Czech Republic). The zeta potentials of a-SEP and a-SEP@LDH aqueous solution were measured in Zeta Potential Analyzer (Brookhaven instrument, zetaPALS, USA) at room temperature. Thermogravimetric analysis (TGA) and derivatives curves (DTG) were tested by SDT Q600 Jupiter Synchronous thermal analyzer (TA, USA) to analyze the thermal degradation behaviour of flame retardants and EP composites. The temperature rose from 30 to 800 °C with a rate of 10 °C/min in N_2 atmosphere. Raman spectroscopy tests were employed to characterize the graphitization degree of all residual char after CCT, using Via (Renishaw, UK) laser Raman spectrometer with a scan range of 800–2000 cm^{-1}. Thermogravimetric infrared spectrometry (TG-FTIR) was carried out on an STA 6000 thermogravimetric analyzer (PerkinElmer, MA, USA) and a Frontier FTIR spectrometer (PerkinElmer, MA, USA) at a heating rate of 20 °C/min under N_2.

LOI values were obtained using JF-3 oxygen index meter (Nanjing Jionglei Instrument Equipment Co., Ltd., China) according to ASTM D2863-97; the sheet dimensions were 100 × 6.5 × 3.2 mm^3. Vertical burning tests (UL-94) were performed using M607 type horizontal vertical burning tester (Qingdao Shanfang Instrument Co., Ltd., China) under ASTM D 3801-2010, and the size of samples was 130 × 13 × 3.2 mm^3. A cone calorimeter test (CCT, FTT) was used to characterize the combustion properties of samples with dimensions of 100.0 mm × 100.0 mm × 4.0 mm under an external heat flux of 50 kW/m^2 according to ISO 5660-1.

Dynamic mechanical analysis (DMA) was carried out using a DMA Q800 apparatus (TA, USA) in a three-point bending pattern. The dimensions of the specimens were 30 × 10 × 4 mm^3. The measuring frequency was 1 Hz, the oscillation amplitude was fixed at 10.0 μm, and the heating rate was 3°C/min from room temperature to 250°C. The tensile properties of all samples were measured using a Microcomputer Control Electronic Universal Testing Machine (ETM105D) at the rate of 2 mm/min, according to GB/T1040.3–2006.

3. Results and discussion

3.1. Characterization of a-SEP@LDH

The phase and composition of a-SEP@LDH were analyzed by XRD and FTIR techniques. The XRD pattern for LDH, as shown in Fig. 1(a), the diffraction peaks at 11.23° and 22.46° are ascribed to the (003) and (006) planes of a typical Ni–Fe LDH structure [50]. The basal spacing is around 7.9 Å calculated from the (003) plane according to Bragg Equation, indicating the NO_3^- as an intercalating anion. In the case of a-SEP@LDH, all the characteristic diffraction peaks related to LDH and a-SEP are maintained, and the intensity of the diffraction peaks of a-SEP is greatly decreased, indicating that the Ni–Fe LDH is successfully self-assembled on the surface of a-SEP. For the FTIR spectrum of a-SEP in Fig. 1(b), the bands at 3674 and 746 cm^{-1} are ascribed to the stretching and bending vibrations of Mg–OH in the octahedral Mg sheet [51]. The bands at 457 and 1384 cm^{-1} as well as the broad absorption band around 1000 cm^{-1} are attributed to the vibration of Si–O–Si within silica tetrahedra [52]. The FTIR spectrum of LDH also shows a sharp band at 1384 cm^{-1} which is originated from the stretching vibration of the interlayer NO_3^- groups [53]. The broad absorption band around 646 cm^{-1} is related to the lattice vibration of Ni–O–Fe [53]. In the FTIR spectra of the three samples, the bands at 3500 and 1630 cm^{-1} belong to the stretching vibration and flexible vibration of O–H of adsorbed water

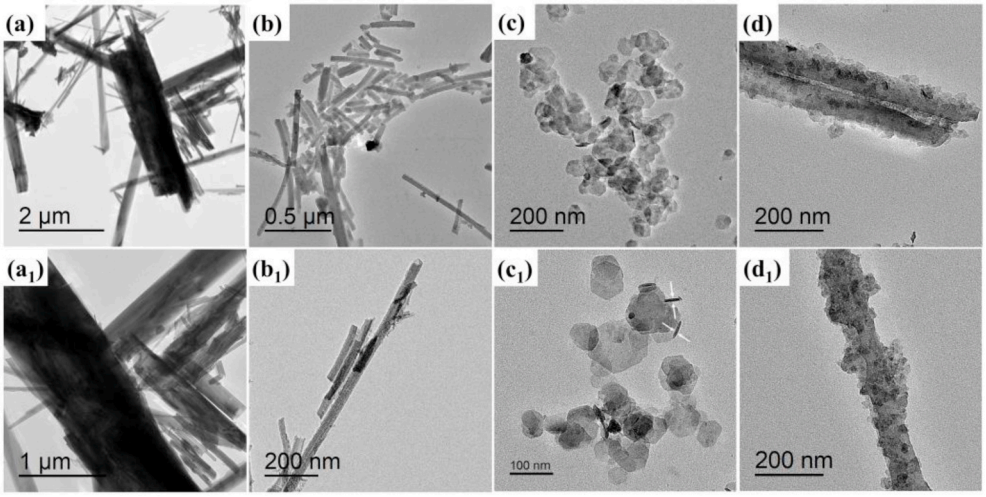

Fig. 2. TEM images of r-SEP (a, a_1), a-SEP (b, b_1), LDH (c, c_1) and a-SEP@LDH (d, d_1).

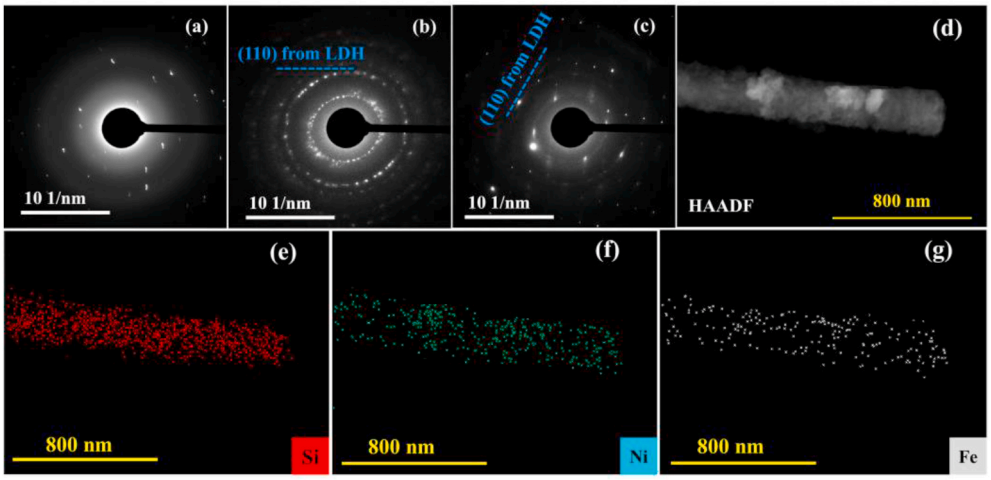

Fig. 3. SAED patterns: (a) a-SEP, (b) LDH, (c) a-SEP@LDH. HAADF and elemental mapping (Si, Ni, Fe) of a-SEP@LDH (d–g).

in structures of both a-SEP and LDH. As for a-SEP@LDH, the characteristic vibration bands of Mg–OH at 3674 and 746 cm^{-1} almost disappear. Noticeably, an obvious broad absorption peak at around 646 cm^{-1} appears, which is attributed to the Ni–O–Fe vibration in LDH. Those changes demonstrate the chemical binding between sepiolite and LDH nanosheets via the partial substitute of Magnesium by Ni and Fe ions except for electrostatic action [54]. Additionally, the vibration bands of Si–O–Si at 457 cm^{-1} and the broad absorption band around 1000 cm^{-1} still exist in a-SEP@LDH, showing that the structure of sepiolite has not been destroyed after the self-assembly of LDH on its surface. Clearly, the absorption band at 1384 cm^{-1} in EP/a-SEP@LDH belongs to the overlapped band for the vibration of Si–O–Si and NO_3^-.

The difference in zeta potential between a-SEP and a-SEP@LDH can also prove the successful preparation of a-SEP@LDH. The surface of a-SEP is negatively charged with a zeta potential of −21.9 mV. Therefore, the self-assembly of positively charged LDH nanosheets is easily

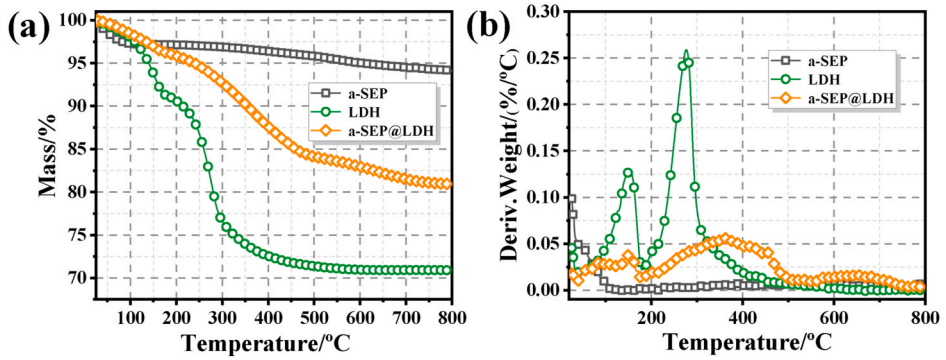

Fig. 4. TG (a) and DTG (b) curves of a-SEP, LDH and a-SEP@LDH in N_2.

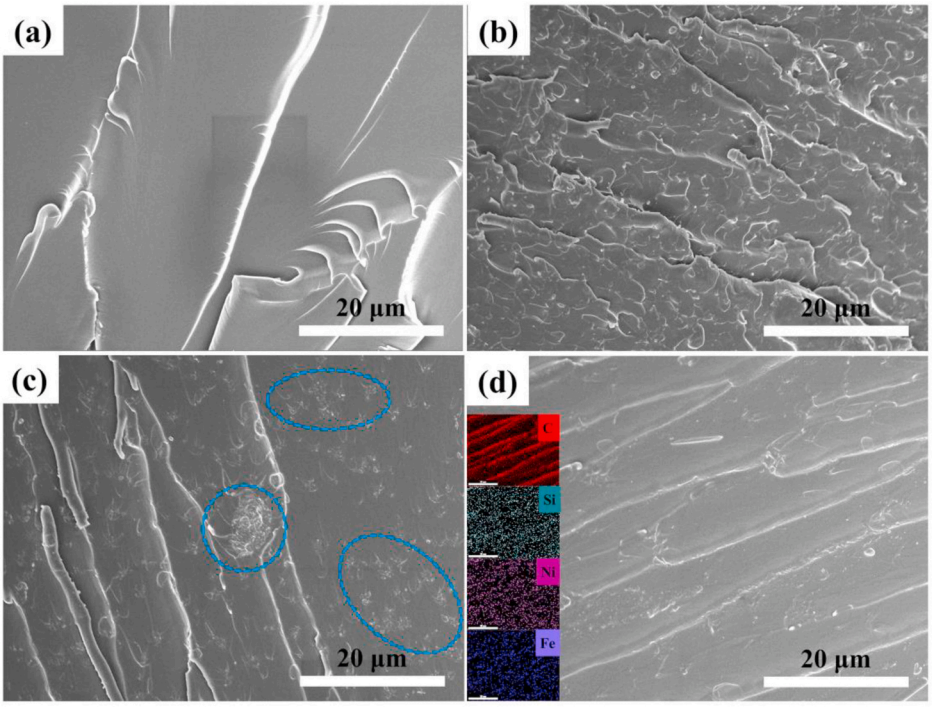

Fig. 5. Fracture surface morphologies of (a) EP, (b) EP/a-SEP, (c) EP/LDH, (d) EP/a-SEP@LDH, the insets are element mapping images (C, Si, Ni, Fe) of EP/a-SEP@LDH.

achieved taking advantage of electrostatic interaction. As expected, the zeta potential of a-SEP@LDH is of +31.2 mV.

The morphologies of r-SEP, a-SEP, LDH and a-SEP@LDH were observed by TEM. As displayed in Fig. 2(a, a_1), the r-SEP shows a fibrous aggregates bundles and its diameter is in a micro size. After the acid treatment of r-SEP, the a-SEP exhibits individual fibers and its diameter is in nano size. LDH shows typical hexagonal lamellar plates with around 10 nm of layer thickness (as shown in Fig. 2(c_1) marked with white arrows) and around 100 nm or larger of the lateral size. Compared with a-SEP, the surface of a-SEP@LDH becomes fairly rough, demonstrating the self-assembled LDH nanosheets on the surface of a-SEP.

To further confirming the structure of a-SEP@LDH, element mapping equipped in TEM was utilized. As shown in Fig. 3(e–g), a-SEP@LDH possesses the characteristic elements of LDH and a-SEP, including Ni, Fe and Si. In the terms of selected area electron diffraction (SAED), a-SEP exhibits dots. After the self-assembled LDH on the surface of a-SEP, the SAED of a-SEP@LDH displays a tendency of diffraction rings. Meanwhile, the (110) plane of LDH can be found [55]. The results of XRD patterns, FTIR, zeta potential, TEM images, SAED and element mapping evidence the successful self-assembly of LDH on the surface of a-SEP.

The TGA and DTG curves of a-SEP, LDH and a-SEP@LDH in N_2 atmosphere are depicted in Fig. 4. The residual weights of a-SEP, LDH and a-SEP@LDH are 94.1%, 70.9% and 80.9% at 800 °C, respectively. Accordingly, the mass percentage of LDH in a-SEP@LDH accounts for 56 wt%. The mass loss of a-SEP mainly is attributed to the loosely bound zeolitic water, hydration water and coordinated water before 800 °C [56]. Regarding LDH, the first decomposition stage starts at room temperature and ends around 200 °C involving the release of absorbed water. Above 200 °C, the decomposition of intercalated NO_3^- anion and dehydroxylation induces the second stage, resulting in the complete destruction of the LDH structure and formation of metal oxides (NiO, $NiFe_2O_4$) [57]. The endothermic decomposition behaviour of a-SEP and LDH with the release of water and inert gases is beneficial to improve flame resistance of EP. Compared with LDH, the a-SEP@LDH exhibits a similar thermogravimetric profile, while the decomposition rate and residual weight of a-SEP@LDH are obviously improved, indicating a-SEP@LDH owns better thermal stability.

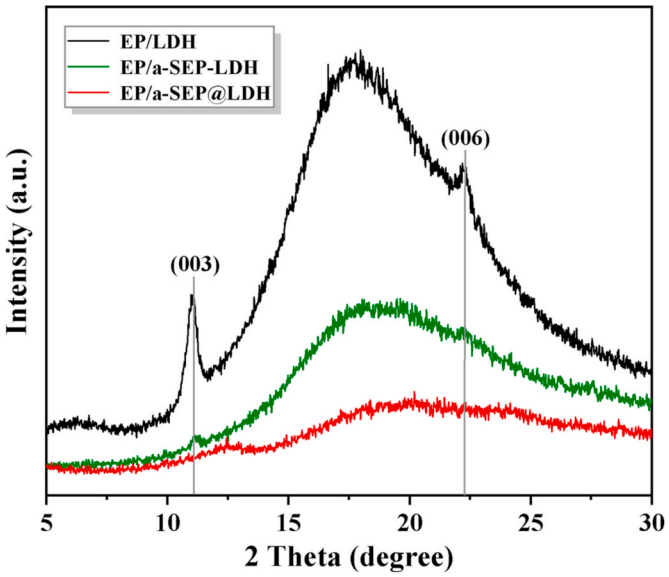

Fig. 6. The XRD patterns of EP/LDH, EP/a-SEP-LDH and EP/a-SEP@LDH.

3.2. Dispersion of a-SEP@LDH in EP matrix

To investigate the dispersion of a-SEP@LDH in EP matrix, the cryo-fractured surfaces of EP and its composites are compared via SEM. As shown in Fig. 5, the fractured surfaces of EP composites are rougher than pure EP. For EP/a-SEP, there is nothing about the aggregation of a-SEP, but a uniform dispersion of a-SEP in EP matrix. In the case of EP/LDH, agglomerates can be clearly observed in Fig. 5(c) and are marked with blue dotted circles, due to the inherent properties of LDH (strong van der Waals interaction). Surprisingly, there is no obvious aggregation of a-

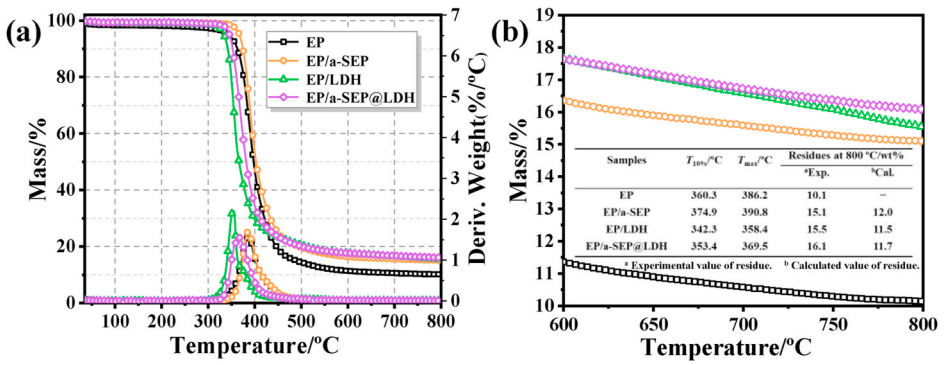

Fig. 7. Thermal analysis of EP and its composites: (a) TG and DTG curves in N_2, (b) the enlarged TG curves among 600–800°C, the $T_{10\%}$, T_{max} and residue (experimental and calculated) at 800 °C for all samples are summarized in insert table.

SEP@LDH in Fig. 5(d), illustrating a well-dispersed a-SEP@LDH in EP matrix. Furthermore, the element mapping images of C, Si, Fe and Ni demonstrate the uniform dispersion of a-SEP@LDH in EP matrix.

In the XRD patterns of EP/LDH and EP/a-SEP-LDH, the (003) and (006) planes are still remained, as shown in Fig. 6. This reflects that the unexfoliated LDH exists in the epoxy matrix. After self-assembled LDH on the surface of sepiolite, the two characteristic diffraction peaks of (003) and (006) planes disappear, which means the LDH is exfoliated. The underlying reason may be the weakened Waals attractions among LDH laminates resulting from the electrostatic interaction between LDH and a-SEP. The XRD data further proves the well-dispersion of a-SEP@LDH in EP matrix. This finding provides a new approach for exfoliating the stacked LDH laminates via electrostatic interaction on a-SEP nanofibers with high specific surface area, which seems to be more convenient than the one assisted with intercalation agent.

3.3. Thermal stability of EP and its composites

The pyrolytic behaviours of EP and EP composites were investigated via TG and DTG under N_2 atmosphere, the corresponding curves and data are shown in Fig. 7. All samples display only one-step decomposition, which is attributed to the decomposition of EP molecular chains [58–60]. EP shows that the temperatures where 10% ($T_{10\%}$) and maximum mass loss (T_{max}) happen are 360.3 and 386.2 °C, respectively, and remains 10.1 wt% residues at 800 °C. With the addition of a-SEP, the related thermal degradation temperatures of EP composite become higher than those of EP, which probably is caused by the high thermal stability and physical barrier effect of a-SEP. It is found that the experimental residue weight of EP/a-SEP is larger than that of EP, as well as more than that of calculated value which follows the linear blended principle. The Si atoms in the tetrahedral sheet of sepiolite are partially replaced by Al atoms (0.04–0.48 per 12 tetrahedra sites), generating the Brønsted acid sites [61]. Therefore, the increased residue weight can be explained by the Brønsted acid sites which are the active sites for aromatization reaction of pyrolytic products of EP molecules, e.g., hydrocarbons [62]. After the introduction of LDH in EP, the $T_{10\%}$ and T_{max} values are dramatically decreased compared to EP, which is responsible for the catalytic decomposed effect of LDH [63]. Meanwhile, the transition metals released from LDH at higher temperature can prompt the formation of a carbonaceous component by catalyzing polyaromatic reaction [17,64], finally resulting in a higher experimental residual weight than the calculated one. As for EP/a-SEP@LDH, the initial decomposed temperature shows earlier than that of EP/a-SEP, which is undoubtedly attributed to the catalytic decomposition effect of LDH on the surface of a-SEP nanofibers. Consequently, due to the dual effect of a-SEP and LDH, as well as the good dispersion of a-SEP@LDH, more char is obtained at the high-temperature stage.

3.4. Combustion behavior of EP and its composites

The combustion behaviors of EP and its composites were investigated via UL-94, LOI and CCT. In terms of UL-94 test, introducing 2.3 wt % a-SEP@LDH endows EP composite a V-1 rating (av-t_1+av-t_2 = 21.6s), which indicates a-SEP@LDH can suppress the fire spread of EP, as depicted in Fig. 8(e). However, the less or excessive weight percentage (2%, 2.6% and 3%) of a-SEP@LDH deteriorates the fire performance of

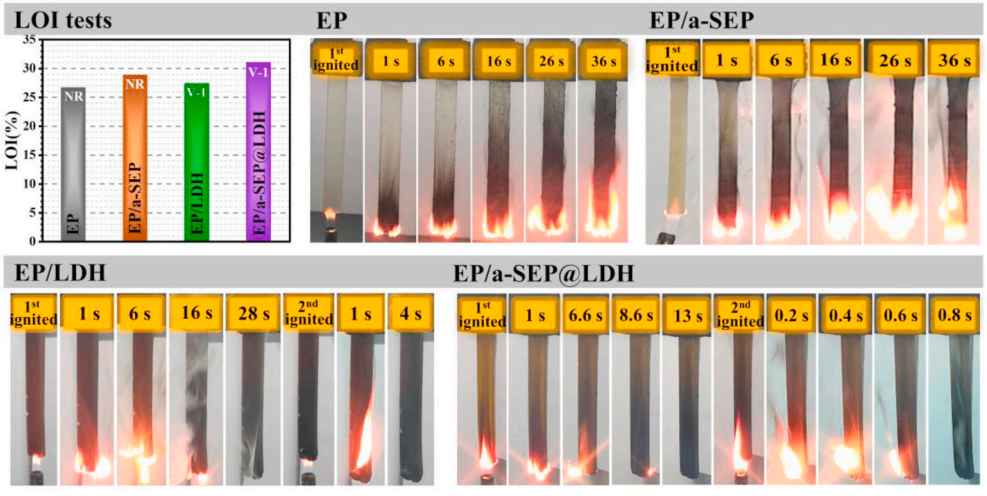

Fig. 8. The results of LOI and the video screenshots of EP and its composites in UL-94 test.

Table 1
The results of EP and its composites in LOI and UL-94 tests.

Samples	LOI (%)	UL-94 test		Dripping	Ratings
		[a]av-t_1/s	[a]av-t_2/s		
EP	26.7	>40.0	-[b]	NO	[c]NR
EP/a-SEP	28.9	31.0	27.0	NO	NR
EP/LDH	27.4	28.0	4.7	NO	V-1
EP/a-SEP@LDH	31.1	16.2	5.4	NO	V-1

[a] Average burning time.
[b] Not recorded.
[c] No rating.

EP composites in UL-94 test, demonstrating that only appropriate amount of a-SEP@LDH can play a fireproof role for EP. Although the dispersion of a-SEP@LDH in EP matrix has been relatively improved, the EP composite still fails to obtain a V-0 rating in the UL-94 test. Two reasons are proposed to explain this phenomenon. As reported in previous literature, nano-materials alone show a limited fire retardant ability in comparison with traditional flame retardants [65]. Additionally, the a-SEP@LDH plays two functions in epoxy: the catalytical decomposition effect and the charring effect. In case of feeding appropriate quantity of a-SEP@LDH, the catalyzing decomposition and charring can be balanced, hence achieving the optimal fire retardancy [66]. The same loading amount of 2.3 wt% of a-SEP@LDH, a-SEP and LDH in EP was chosen to further assessment by UL-94, LOI and CCT. For EP, the flame rapidly spreads along the tested spline and hardly extinguishes after the first ignition, as shown in Fig. 8(b), determining an NR rating. EP/a-SEP fails to pass the UL-94 test. Although LDH also assigns V-1 rating to EP composite, the av-t_1 of EP/LDH is longer than that of EP/a-SEP@LDH. For EP/a-SEP-LDH, the av-t_1 and av-t_2 are 15.0 s and beyond 30 s (in Figure S1), respectively. Apparently, the flame-retardant efficiency of EP/a-SEP-LDH is lower than that of EP/a-SEP@LDH, which is mainly ascribed to the worse dispersion state of fillers. In the LOI test, as shown in Table 1, adding 2.3 wt% a-SEP in EP increases the LOI value to 28.9% from 26.7% of EP. The LOI value of EP/LDH is slightly increased to 27.4%. However, EP/a-SEP@LDH displays a significantly improved LOI value of 31.1%. The improved fire performances of EP/a-SEP@LDH in UL-94 and LOI tests take advantage of the dual effect of a-SEP and LDH and the well dispersion of a-SEP@LDH in EP matrix.

CCT has been frequently carried out to reproduce the fire response of polymers in an approximate real combustion condition and following this to judge the fire behaviour of materials [67]. In terms of CCT, various characteristic parameters, including time to ignition (TTI), the peak of heat release rate (pHRR), average effective heat combustion (av-EHC), total smoke production (TSP), average specific extinction area (av-SEA) and carbon monoxide production (COP) are summed up in Table 2. The corresponding curves of heat release rate (HRR), TSP, COP and the CO/CO_2 ratio versus time are illustrated in Fig. 9. The trends of TTI values for EP and EP composites are consistent with the results of TG tests. The TTI value of EP/a-SEP@LDH is lower than those of EP and EP/a-SEP, which is induced by the catalytic decomposition effect of

Table 2
Cone calorimetric data of the testing samples.

Samples	TTI (s)	pHRR (kW/m^2)	av-EHC (MJ/kg)	TSP (m^2)	av-SEA (m^2/kg)	Total COP(g)	Residue (wt%)
EP	58 ± 1	1077.8 ± 11.0	24.1 ± 0.1	45.4 ± 1.1	871.0 ± 32.7	7.9 ± 0.2	12.0 ± 0.2
EP/a-SEP	59 ± 1	889.9 ± 9.8	22.9 ± 0.5	48.1 ± 1.6	954.4 ± 13.9	8.5 ± 0.1	9.9 ± 0.1
EP/LDH	47 ± 1	869.2 ± 8.8	21.9 ± 0.1	39.0 ± 0.3	666.5 ± 8.2	7.1 ± 0.1	12.3 ± 0.1
EP/a-SEP@LDH	48 ± 1	835.4 ± 9.0	17.0 ± 0.7	38.1 ± 0.3	567.4 ± 9.0	5.9 ± 0.1	14.9 ± 0.2

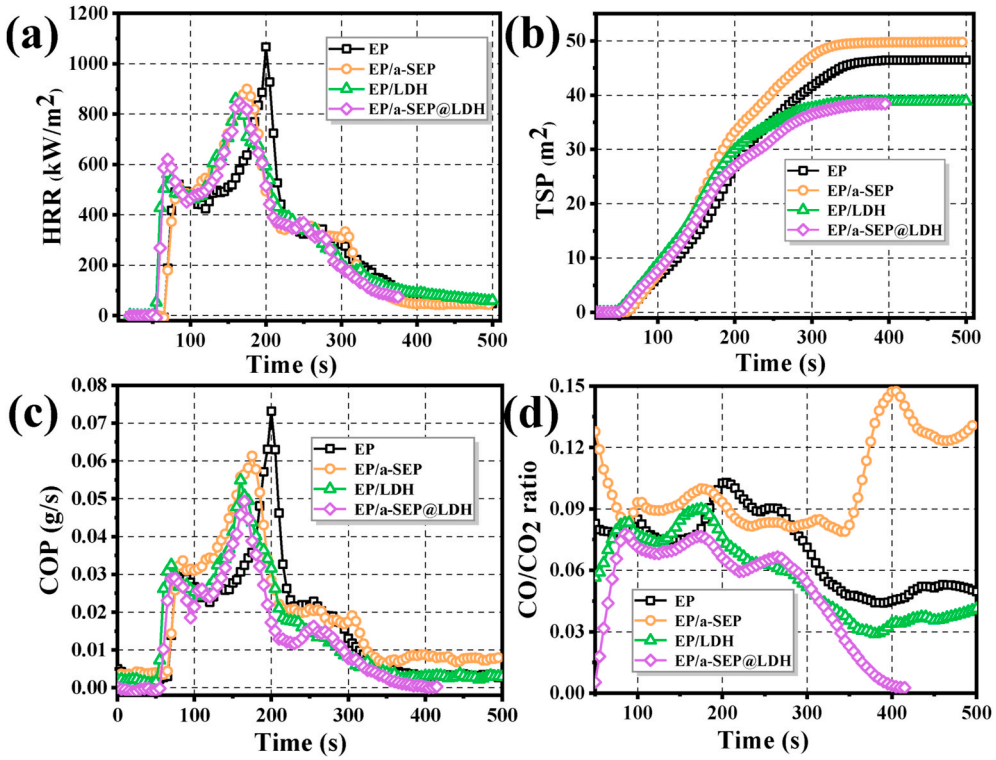

Fig. 9. HRR (a), TSP (b), COP and CO/CO_2 plots as a function of time for EP and its composites.

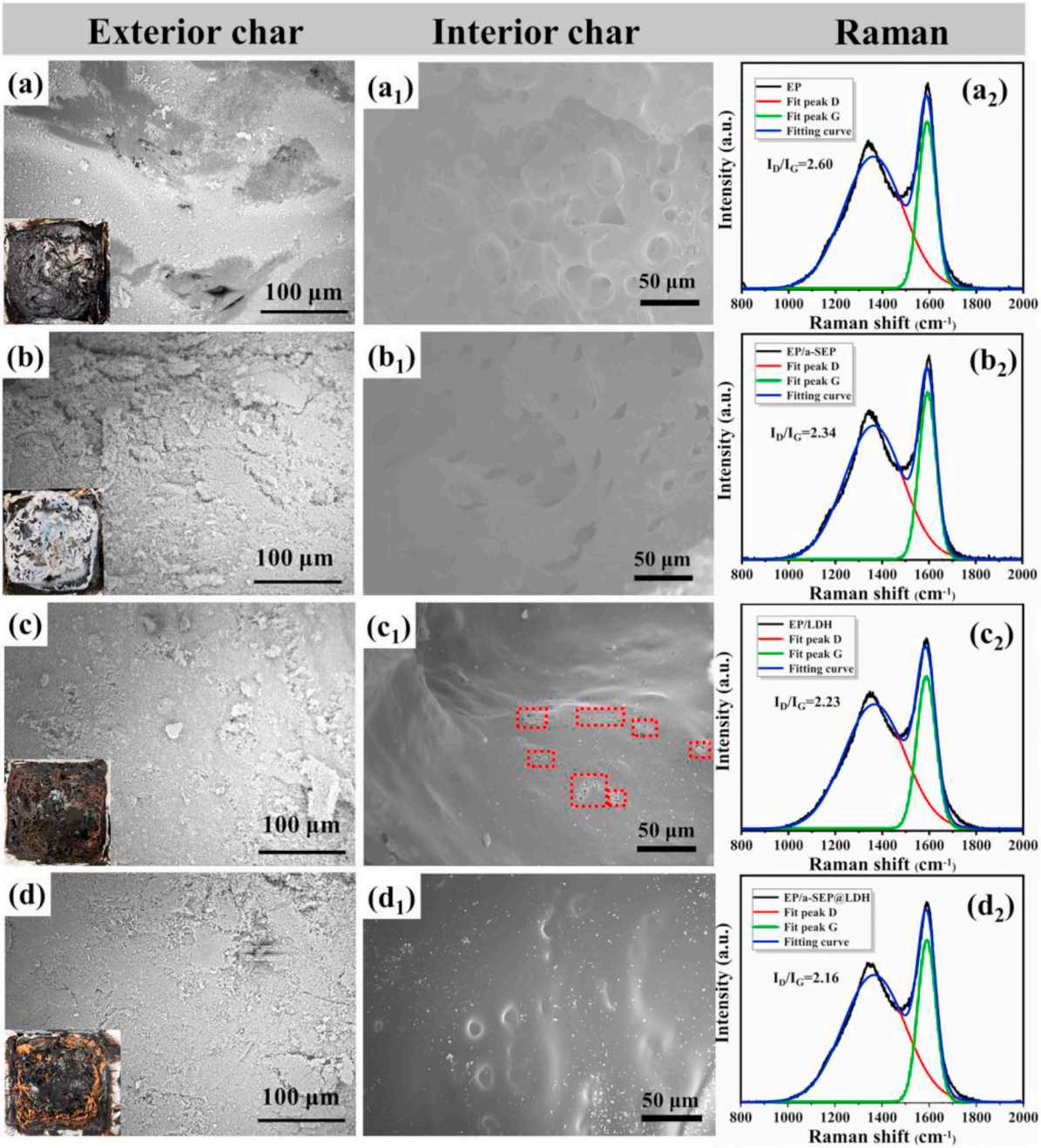

Fig. 10. The char residues of all samples collected from CCT were studied by SEM and Raman spectra: (a, a_1, a_2) EP, (b, b_1, b_2) EP/a-SEP, (c, c_1, c_2) EP/LDH, (d, d_1, d_2) EP/a-SEP@LDH. The insets in (a–d) are the digital photos of char residue after CCT.

LDH. The pHRR value of EP/a-SEP@LDH composite is obviously decreased by 21% compared with that of EP, due to the improved quality of char. Additionally, the av-EHC of various EP composites is gradually decreased with the introduction of flame retardants. In particular, the av-EHC of EP/a-SEP@LDH is reduced to 17.0 from 24.1 of EP, which means less-flammable volatile products in the gas phase [68]. This could be explained by the barrier effect of high-quality char layer and diluting effect of the released inert gases from both a-SEP and LDH (as discussed in section 3.1.). Interestingly, the TSP of EP/a-SEP is increased compared with EP, which probably is induced by the further decomposition of unstable char [69,70]. As carefully checked the TSP plots of all samples, the growth trend of TSP curves for EP/LDH and EP/a-SEP@LDH is descending after 235 s in comparison with EP/a-SEP, indicating that the addition of a-SEP alone is not enough to form a stable char layer. Additionally, the COP and CO/CO_2 curves of EP/a-SEP display the same trend as TSP after 235 s, which does identify that the decomposition of the unstable char of EP/a-SEP results in the increased TSP, COP and CO/CO_2. Noticeably, the final TSP values of EP/LDH and EP/a-SEP@LDH are mostly the same. However, the TSP curve of EP/a-SEP@LDH is obviously lower than that of EP/LDH system from 200 to 235 s. These variations mirror the synergistic fire-retarding effect between sepiolite and LDH during combustion, which is helpful to strengthen the char residue and prevent the further decomposition of char, resulting in a higher char yield of 14.9 wt%. Reasonably, the variation tendencies of av-SEA of various EP composites are in accordance with TSP. Particularly, the av-SEA of EP/a-SEP@LDH is reduced by 35% compared to EP. Due to the decomposition of the unstable char of EP/a-SEP, the char residual weight of EP/a-SEP is lower than that of

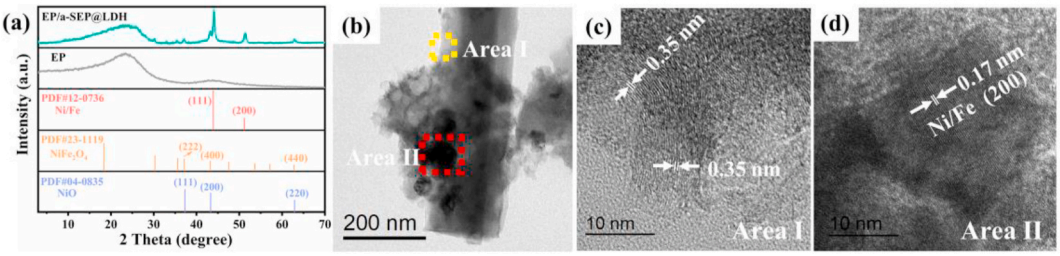

Fig. 11. The XRD patterns of char residue for EP and EP/a-SEP@LDH (a). The low magnification (b) and high-resolution magnification (c, d) images of char residue for EP/a-SEP@LDH.

EP. Combining the dual effect of a-SEP and LDH, the EP/a-SEP@LDH owns the highest char residual weight than other samples. Usually, the CO, as a kind of toxic gases, should also be concerned [71]. The total COP of EP/a-SEP@LDH is significantly decreased by 25.3% in contrast to EP. Meanwhile, the EP/a-SEP@LDH exhibits the lowest CO/CO_2 ratio during CCT in comparison with EP/a-SEP and EP/LDH composites. The remarkably reduced CO/CO_2 ratio probably is caused by the catalytic oxidation of the LDH in a-SEP@LDH and the barrier effect of high-quality char. In respect of UL-94, LOI and CCT, the EP/a-SEP@LDH shows better fireproof performance and lower toxicity than other samples.

3.5. Fire-retardant mechanism

To explore the potential fire retarding mechanism, the char residues of EP and EP composites after CCT were studied by SEM, TEM, Raman spectra and XRD. As shown in Fig. 10(a–d), some obvious holes can be found in the exterior surface of the char residue for EP. EP/a-SEP owns a very loosely exterior char residue, while EP/LDH and EP/a-SEP@LDH possess relatively compact and continuous ones, especially for EP/a-SEP@LDH. Concerning the interior char residue (Fig. 10(a_1-d_1)), some broken bubbles and stomas can be observed in EP. This type of char cannot effectively hinder the transmission of heat and oxygen. After incorporation of a-SEP, the interior char layer of EP composite shows many holes, which is ascribed to the further decomposition of the unstable char during combustion. Surprisingly, the interior char layers of EP composites containing LDH become much continuous and compact than EP and EP/a-SEP, especially for EP/a-SEP@LDH system (the interior char of EP/LDH still owns some small holes marked with red dotted boxes in Fig. 10(c_1)). The greatly improved char quality of EP/a-SEP@LDH system may mainly thank to the catalytic crosslinking effect of LDH and the solidification of a-SEP nanofibers. It is supposed that the metal oxides or metal element released from LDH can catalyze the polyaromatic reaction of the pyrolytic products of EP molecules on the surface of sepiolite nanofibers, and induce a high-viscosity melt, resulting in the formation of high-quality char solidified by sepiolite nanofibers [72]. Raman spectroscopy was used to further study the quality of char residues after CCT. As shown in Fig. 10(a_2-d_2), all the samples show a D band at 1349 cm^{-1} and a G band at 1590 cm^{-1}. For EP/a-SEP@LDH composite, the ratio of the integrated peak area of the D and G band, namely I_D/I_G, is the lowest than those of counterparts. Generally, a lower I_D/I_G value means more graphite carbon formed in char residue [73].

The char residue of EP/a-SEP@LDH was ultrasonically dispersed in ethanol and then further analyzed via TEM, as shown in Fig. 11(b, c, d). As discussed above, sepiolite remains the nanofiber shape and is coated by some graphene layers on its surface. It is found that the lattice fringes of graphene are well ordered, meaning fewer defects in the graphite planes. The XRD pattern of char residue of EP/a-SEP@LDH, as shown in Fig. 11(a), shows the existence of $NiFe_2O_4$ (PDF#23–1119), NiO

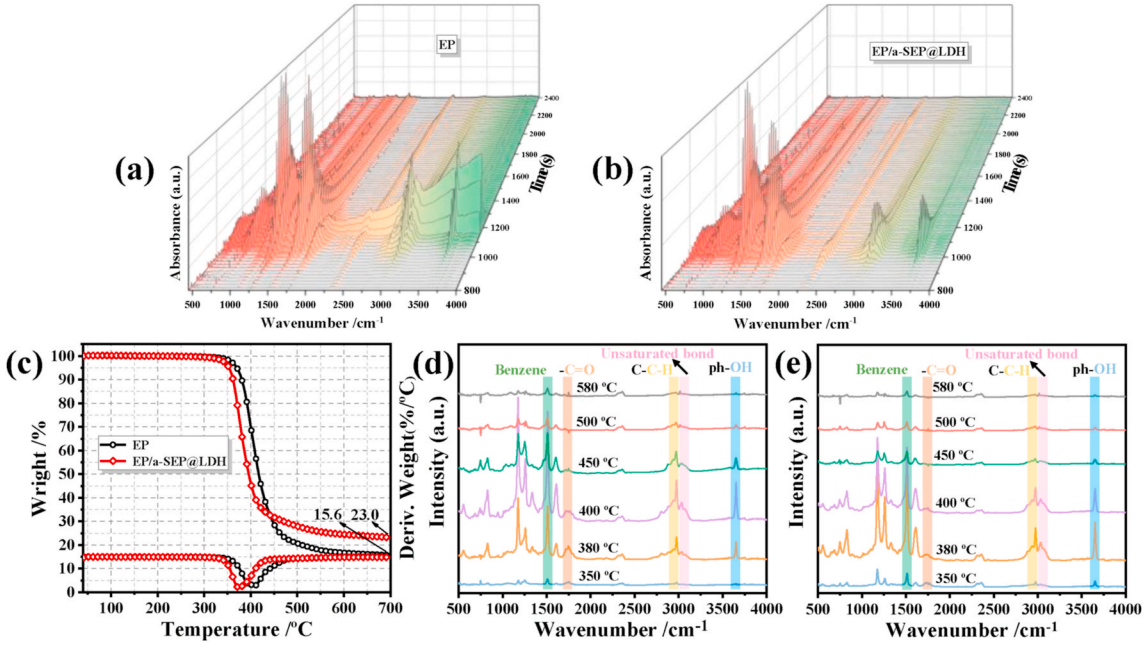

Fig. 12. The 3D FTIR spectra of EP (a) and EP/a-SEP@LDH (b). The TG and DTG curves of EP and EP/a-SEP@LDH from TG-FTIR test (c). FTIR spectra of volatile products for EP (d) and EP/a-SEP@LDH (e) at different temperatures.

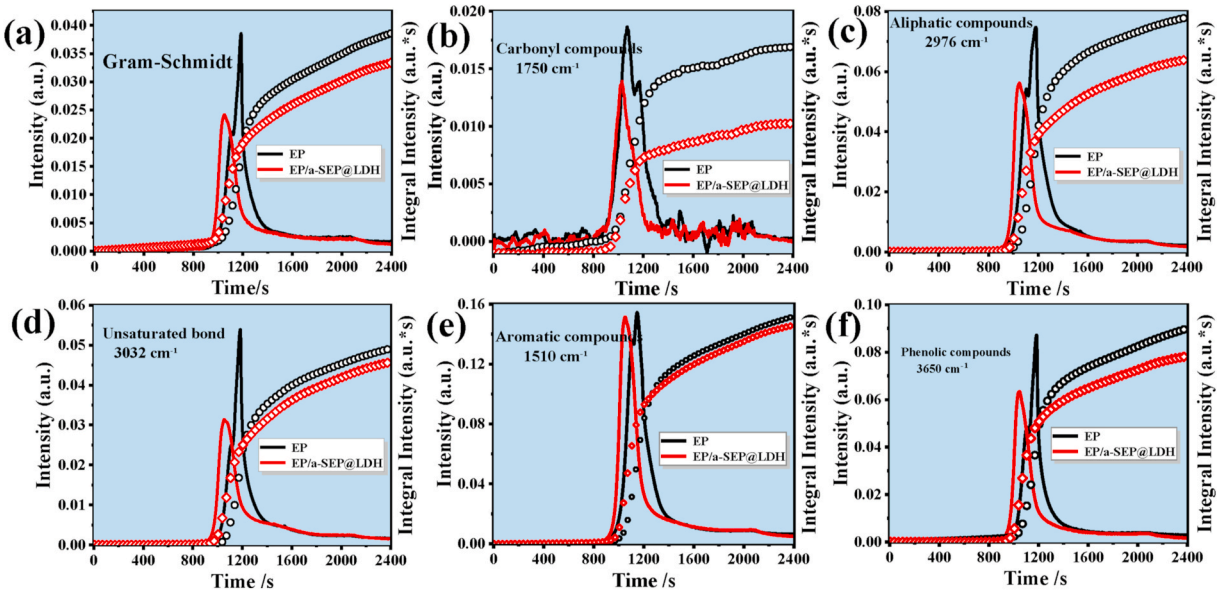

Fig. 13. Absorbance and integral curves of volatile products for EP and EP/a-SEP@LDH: (a) Gram-Schmidt curves, (b) carbonyl compounds, (c) aliphatic compounds, (d) unsaturated bond, (e) aromatic compounds, (f) phenolic compounds.

(PDF#04–0835), Ni/Fe alloy (PDF#12–0736) and sepiolite. Besides, the (002) diffraction of graphite at approximately 25° can be found both in EP and EP/a-SEP@LDH. The lattice fringes of (200) plane in Ni/Fe alloy catalyst is observed in Fig. 11(d) [74]. The Ni/Fe alloy catalyst is derived from the reduction of partial metal oxides induced by reductants, e.g., CO (NiO and $NiFe_2O_4$, $Fe^{3+}\rightarrow Fe^{2+}\rightarrow Fe$, $Ni^{2+}\rightarrow Ni$) [37], and can catalyze the formation of carbonaceous components [15]. Meanwhile, sepiolite and metal oxides originated from LDH can act as physical reinforcement for the char residue. Therefore, the char residue of EP/a-SEP@LDH shows more integrity than other samples.

TG-FTIR test was further conducted to investigate the effect of a-SEP@LDH on the pyrolysis mode and gaseous phase behaviour of EP. The $T_{5\%}$ (the temperature where 5% mass loss happens) of EP/a-SEP@LDH is earlier than that of EP (368 °C) in Fig. 12(c), and the absorbance intensities of all bands in the FTIR spectrum of EP/a-SEP@LDH are stronger than those of EP at 350 °C. This indicates the catalytic decomposition effect of a-SEP@LDH on EP. Additionally, the T_{max} of EP/a-SEP@LDH shows at 380 °C, while the EP at approximate 400 °C. Therefore, as shown in Fig. 12(a, b, d, e), the absorbance intensities of all bands of both EP and EP/a-SEP@LDH gradually become weak after their T_{max}, especially for EP/a-SEP@LDH. Consequently, the char residual weight of EP/a-SEP@LDH is 23.0% and higher than that of EP (15.6 wt%), indicating the catalytic charring effect of a-SEP@LDH.

EP and EP/a-SEP@LDH exhibit similar pyrolysis gases at different thermal degradation temperatures, as shown in Fig. 12(d and e). The main gaseous products include aromatics (1510 cm^{-1}), carbonyl compounds (1750 cm^{-1}), aliphatic compounds (2976 cm^{-1}), unsaturated bond (3032 cm^{-1}) and phenolic compounds (3650 cm^{-1}). More importantly, with the addition of a-SEP@LDH, both the peak absorbance intensity and integral intensity of Gram-Schmidt curve for EP composite are decreased compared to those of EP as shown in Fig. 13(a). This difference is ascribed to the barrier effect of high-quality char residue and thus less-flammable volatiles are released in the gaseous phase. More specifically, as depicted in Fig. 13(b), both the peak absorbance

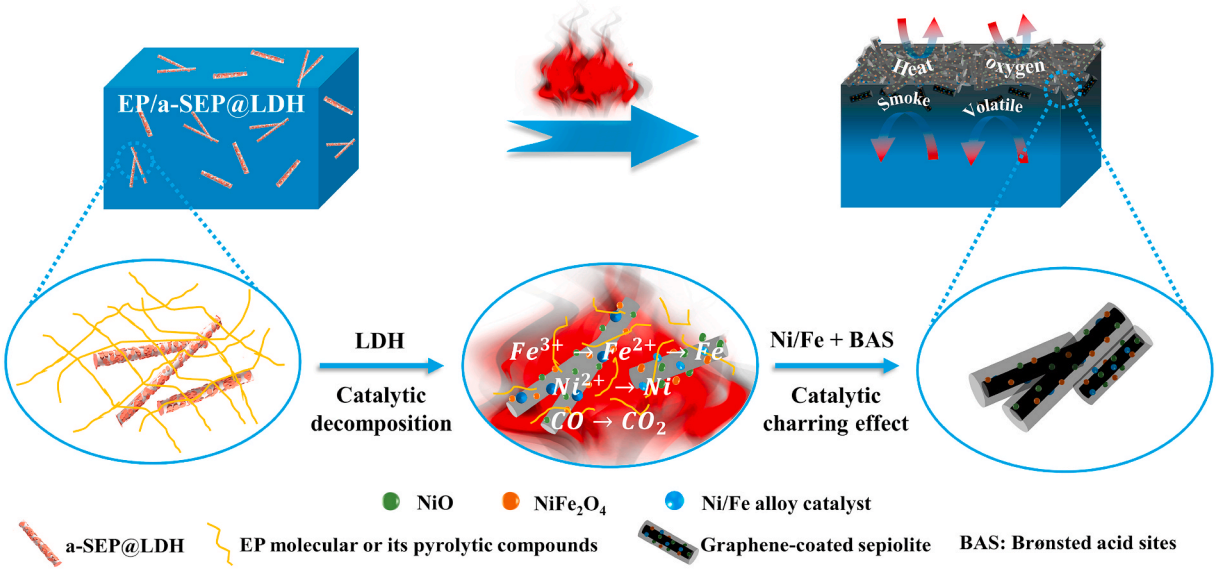

Scheme 2. The flame retardant mechanism of EP/a-SEP@LDH.

Table 3
The characteristic data of EP and EP composites collected from tensile and DMA tests.

Samples	Stress at break (MPa)	Elongation at break (%)	E' (MPa) at 40°C	E″ peak (MPa)	T_g (°C)	ρ (mol/m^3)
EP	64.9 ± 6.3	7.2 ± 0.5	3128	321.5	157.6	1380
EP/a-SEP	66.5 ± 6.1	6.9 ± 0.9	4820	341.8	164.6	2420
EP/LDH	68.5 ± 6.2	6.9 ± 0.5	5811	341.1	166.7	2520
EP/a-SEP@LDH	78.9 ± 1.0	8.4 ± 0.2	3965	286.4	174.1	1550

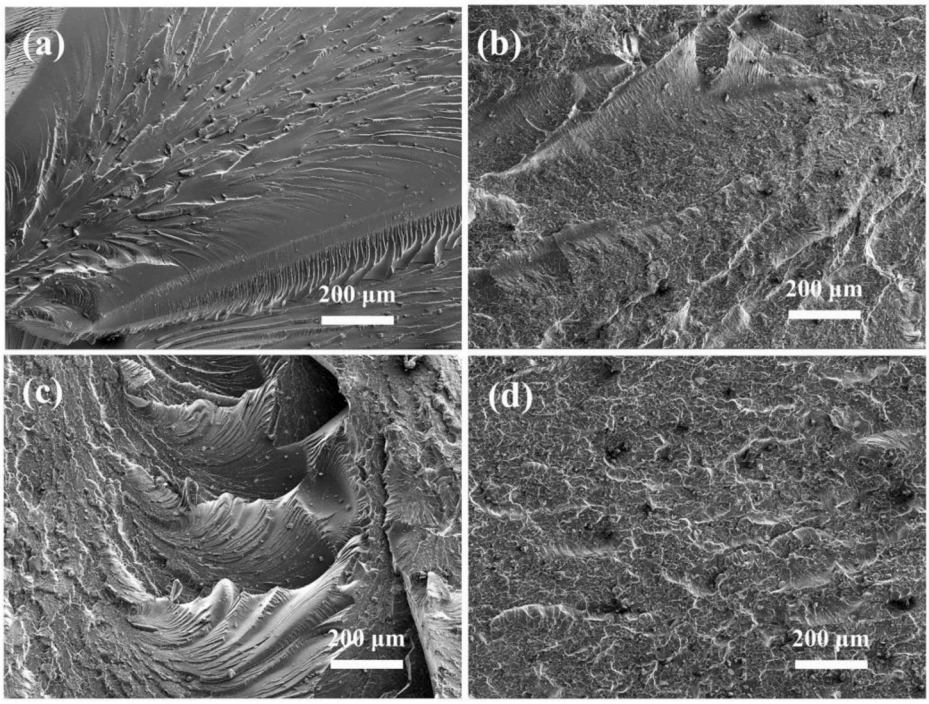

Fig. 14. SEM fracture surfaces after tensile tests of EP (a), EP/a-SEP (b), EP/LDH (c) and EP/a-SEP@LDH (d).

intensity and integral intensity of carbonyl compounds for EP/a-SEP@LDH are greatly decreased. The carbonyl compounds originated from the cleavage and rearrangement of acid anhydride in bisphenol A epoxy resin [75]. Therefore, the decreased carbonyl compounds of EP/a-SEP@LDH system means the underlying epoxy is well protected by the high-quality char during combustion. Upon with catalytic charring effect of a-SEP@LDH, the decreased release of aliphatic, aromatic, phenolic and unsaturated bond compounds is a shred of cogent evidence. As discussed in section 3.3, the Brønsted acid sites in sepiolite can catalyze the aromatization reaction of hydrocarbons; the Ni/Fe alloy catalyst can further catalyze the polyaromatic reaction on the surface of sepiolite based on C–C and C–N coupling reaction [17,76]. In a nutshell, the improved fireproofing properties of EP/a-SEP@LDH composite takes advantage of the synergistic effect of a-SEP and LDH.

Based on the above investigation of char residues after CCT for EP and EP/a-SEP@LDH, as well as the difference of pyrolysis products via TG-FTIR, the mechanism of fire retardance and smoke suppression of EP/a-SEP@LDH system is mainly attributed to the follows: a) physical solidified char residue by sepiolite nanofibers; b) catalytic charring effect of Ni/Fe alloy and Brønsted acid sites (Scheme 2). In detail, under fire attack, firstly, the LDH on the surface of sepiolite catalyzes the decomposition of EP accompanying with the formation of metal oxides. Meanwhile, the partial metal oxides can be reduced by CO during combustion, leading to the formation of Ni/Fe alloy catalyst. Then, the pyrolytic compounds including aliphatic, unsaturated bond, aromatic and phenolic are jointly catalyzed by Ni/Fe alloy catalyst and Brønsted acid sites in sepiolite into carbonaceous components which are located on the surface of sepiolite, leading to a high-viscosity melt. Consequently, the high-viscosity melt induces the connection of sepiolite structures coated with carbonaceous components, forming a high-quality char. The formed high-quality char is conducive to suppressing the release of heat and smoke (the reduced pHRR, TSP and CO/CO_2 in CCT).

3.6. Mechanical properties of EP and its composites

The tensile and DMA tests were used to evaluate the mechanical strength and thermal resistance of EP and EP composites, and corresponding results are listed in Table 3. In the terms of tensile test, compared with 64.9 ± 6.3 MPa of EP, the tensile strength of EP/a-SEP and EP/LDH have been enhanced to 66.5 ± 6.1 and 68.5 ± 6.2 MPa, respectively. After LDH self-assembled on the surface of a-SEP, the tensile strength of EP/a-SEP@LDH is increased to 78.9 ± 1.0 MPa and its elongation at break is increased from 7.2 ± 0.5% of EP to 8.4 ± 0.2%. The improved tensile property of EP/a-SEP@LDH reflects the good dispersion of a-SEP@LDH (as discussed in section 3.2).

To investigate the strengthening mechanism, the SEM images of the fracture surface for all samples are compared, as shown in Fig. 14. The fracture surface of the EP is smooth with plenty of "radiation-like" patterns, which represents the rapid crack propagation [77]. For EP composites, the fracture surfaces become rough in different degree, especially for EP/a-SEP@LDH. This is ascribed to the changed direction of crack propagation induced by flame retardants, indicating the abundant energy requirement of crack propagation [78]. Therefore, the enhanced mechanical strength of EP composites is explained by the dissipated fracture energy in the presence of flame retardant filler.

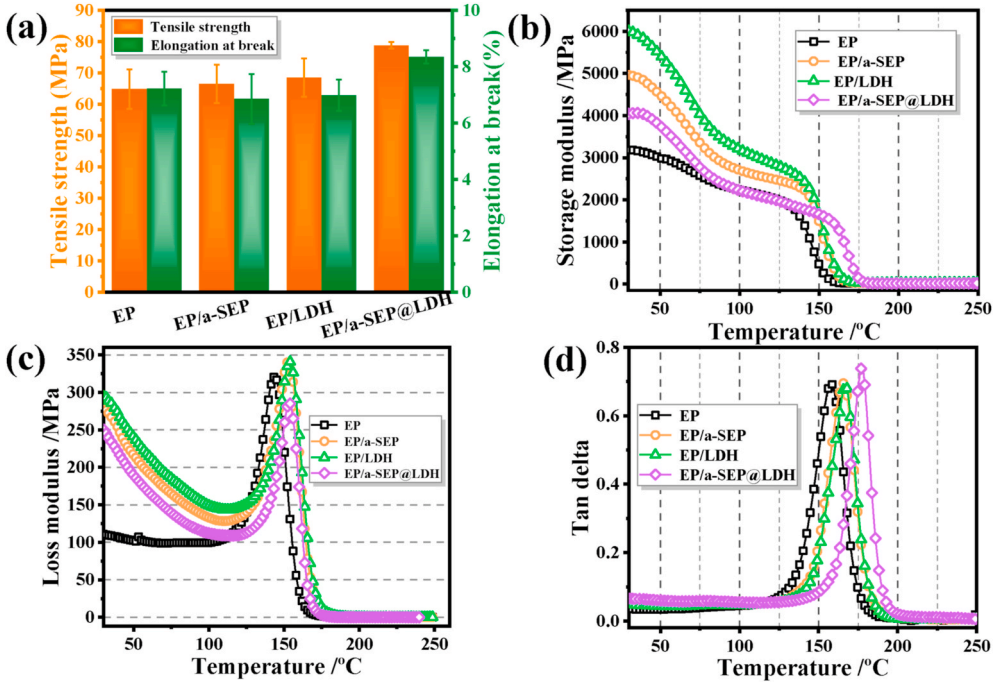

Fig. 15. The results of tensile tests of EP and its composites (a). The results of the DMA test: (b) storage modulus, (c) loss modulus and (d) tanδ.

The dynamic mechanical study provides the information of the storage modulus (E′), loss modulus (E″) and dissipation factor (tanδ) within a certain temperature range for polymer composites. E′ represents the elastic behaviour and energy storage of the material under cyclic deformation. E″ is a measure of the viscous response of the material and reflects the friction among the polymer chains. The tanδ characterizes the damping behaviour of material and the peak of tanδ is referred to the glass transition temperature (T_g). The E′ of EP/a-SEP and EP/LDH are higher than that of EP in the glassy state (Fig. 15(b)). Unexpectedly, the E′ of EP/a-SEP@LDH is decreased in comparison with EP/a-SEP and EP/LDH. Excitedly, the E′ of EP/a-SEP@LDH is higher than that of EP. The cross-linking density (ρ) has a profound effect on the mechanical strength and T_g of epoxy and thus the ρ of EP and its composites were calculated according to this equation [79]: $\rho = G^{'}/\ 3RT$. The parameters $G^{'}$, R and T are the storage modulus of epoxy at T_g + 40 °C, the gas constant (8.314 J mol^{-1} K^{-1}) and the temperature at T_g + 40 °C, respectively. As shown in Table 3, the order of ρ for EP and EP composites are as follows: EP/LDH > EP/a-SEP > EP/a-SEP@LDH > EP. The increased cross-linking density of EP composites may be ascribed to the Lewis acid action in both LDH and sepiolite. The Lewis acid can catch the lone-pair electron of oxygen in epoxide ring and thus drive the ring open reaction [80]. After the positively charged LDH self-assembled on the negatively charged sepiolite, the charge transfer may happen between sepiolite and LDH [81] and thus the Lewis acid action is weakened, resulting in a lower ρ of EP/a-SEP@LDH than those of EP/LDH and EP/a-SEP. Noticeably, the order of storage modulus at 40 °C is the same as the ρ. Apparently, the modulus of EP composites in glassy state is mainly affected by cross-linking density. The T_g of EP composites all displays an increased value in comparison with that of EP. As reported in the previous literature, the inorganic fillers can act as a physical cross-link point which has an more important impact than cross-linking density on the T_g of epoxy at high temperature [82]. Therefore, the improved dispersion of a-SEP@LDH (in Figs. 5 and 6) will play a better physical cross-linking role, the T_g of EP/a-SEP@LDH is significantly increased to 174.1°C from 157.6°C of EP, as shown in Fig. 15(d). Thus, the movement of EP chain segment is restricted. The decreased E″ for EP/a-SEP@LDH demonstrates the restriction of EP chain and thus alleviates the friction among them.

4. Conclusions

Aiming to improve the dispersion of Ni–Fe LDH in EP matrix, sepiolite nanofibers were used as a supporter to synthesize a-SEP@LDH via self-assembly. It is found that weakening the electrostatic interaction among LDH laminates can be realized by self-assembly between negatively charged a-SEP and positively charged LDH, which facilitates the exfoliation of LDH laminates and uniform dispersion of a-SEP@LDH in EP matrix. With the addition of 2.3 wt% a-SEP@LDH, the composite owns an enhanced flame retardance, reflecting in an LOI value of 31.1%, a V-1 rating, 21% reduction of pHRR and decreased 16.0% TSP. The a-SEP@LDH works for the improved fire safety of EP composite in two forms: a) sepiolite acting as a solidification role for char; b) the catalytic charring effect of both Ni/Fe catalyst and Brønsted acid sites. Therefore, high-quality char leads to the reduced both pHRR and TSP and partial metal oxides reduced into Ni/Fe consumes the CO. Especially, the tensile strength and T_g of EP/a-SEP@LDH are enhanced simultaneously. Through analyzing the SEM of fracture surface after the tensile test of EP/a-SEP@LDH, the increased tensile strength benefits from the dissipated fracture energy effect of a-SEP@LDH. Meanwhile, a-SEP@LDH can act as a physical cross-link point to increase the T_g of the EP composite. Therefore, it is an effective way for simultaneously improving the fire retardance, mechanical strength and thermal resistance of EP composite by utilizing a-SEP@LDH filler.

Author statement

Haijun Zhang: Conceptualization, Methodology, Formal analysis, Data curation, Writing - original draft, Project administration. **Xiaoping Hu**: Conceptualization, Methodology, Resources, Data curation, Writing - review & editing, Supervision. **Yingru Liu**: Validation, Investigation. **Suhua Zhang**: Conceptualization, Software. **Zhenzhong Wu**: Conceptualization, Investigation.

Declaration of competing interest

The authors declare that they have no known competing financial interests or personal relationships that could have appeared to influence

the work reported in this paper.

Acknowledgements

This work was financially supported by the National Natural Science Foundation of China (No. 51673160; 51973178), and Postgraduate Innovation Fund Project by Southwest University of Science and Technology (No. 19ycx0027).

Appendix A. Supplementary data

Supplementary data to this article can be found online at https://doi.org/10.1016/j.compositesb.2021.108857.

References

[1] Jin FL, Li X, Park SJ. Synthesis and application of epoxy resins: a review. J Ind Eng Chem 2015;29:1–11.
[2] Wang PJ, Liao DJ, Hu XP, Pan N, Li WX, Wang DY, Yao Y. Facile fabrication of biobased P-N-C-containing nano-layered hybrid: preparation, growth mechanism and its efficient fire retardancy in epoxy. Polym Degrad Stabil 2019;159:153–62.
[3] Fu T, Guo DM, Chen L, Wu WS, Wang XL, Wang YZ. Fire hazards management for polymeric materials via synergy effects of pyrolysates-fixation and aromatized-charring. J Hazard Mater 2020;389:122040.
[4] Muriel R, Sebastian W, Manfred D. Recent developments in halogen free flame retardants for epoxy resins for electrical and electronic applications. Materials 2010;3:4300–27.
[5] Velencoso MM, Battig A, Markwart JC, Schartel B, Wurm FR. Molecular firefighting-how modern phosphorus chemistry can help solve the challenge of flame retardancy. Angew Chem Int Ed 2018;57:10450–67.
[6] Jin SL, Qian LJ, Qiu Y, Chen YJ, Xin F. High-efficiency flame retardant behavior of bi-DOPO compound with hydroxyl group on epoxy resin. Polym Degrad Stabil 2019;166:344–52.
[7] Xie WQ, Huang SW, Liu SM, Zhao JQ. Phosphorus-based triazine compound endowing epoxy thermosets with excellent flame retardancy and enhanced mechanical stiffness. Polym Degrad Stabil 2020;180:109293.
[8] Jian RK, Ai YF, Xia L, Zhao LJ, Zhao HB. Single component phosphamide-based intumescent flame retardant with potential reactivity towards low flammability and smoke epoxy resins. J Hazard Mater 2019;371:529–39.
[9] Zou JH, Duan HJ, Chen YS, Ji S, Cao JF, Ma HR. A P/N/S-containing high-efficiency flame retardant endowing epoxy resin with excellent flame retardance, mechanical properties and heat resistance. Compos B Eng 2020;199:108228.
[10] Cheng JW, Duan HJ, Yang S, Wang J, Zhang QQ, Ding GP, Hu YF, Huo SQ. A P/N-containing flame retardant constructed by phosphaphenanthrene, phosphonate, and triazole and its flame retardant mechanism in reducing fire hazards of epoxy resin. J Appl Polym Sci 2020;137:e49090.
[11] Yang S, Huo SQ, Wang J, Zhang B, Wang JS, Ran SY, Fang ZP, Song PA, Wang H. A highly fire-safe and smoke-suppressive single-component epoxy resin with switchable curing temperature and rapid curing rate. Compos B Eng 2021;207:108601.
[12] Xiao YL, Jin ZY, He LX, Ma SC, Wang CY, Mu XW, Song L. Synthesis of a novel graphene conjugated covalent organic framework nanohybrid for enhancing the flame retardancy and mechanical properties of epoxy resins through synergistic effect. Compos B Eng 2020;182:107616.
[13] Gu HB, Ma C, Gu JW, Guo J, Yan XR. An overview of multifunctional epoxy nanocomposites. J Mater Chem C 2016;4:5890–906.
[14] Li WX, Zhang HJ, Hu XP, Yang WX, Cheng Z, Xie CQ. Highly efficient replacement of traditional intumescent flame retardants in polypropylene by manganese ions doped melamine phytate nanosheets. J Hazard Mater 2020;398:123001.
[15] Huo SQ, Song PA, Yu B, Ran SY, Chevali VS, Liu L, Fang ZP, Wang H. Phosphorus-containing flame retardant epoxy thermosets: recent advances and future perspectives. Prog Polym Sci 2021;114:101366.
[16] Kiliaris P, Papaspyrides CD. Polymer/layered silicate (clay) nanocomposites: an overview of flame retardancy. Prog Polym Sci 2010;35:902–58.
[17] Li Z, Liu ZQ, Dufosse F, Yan LK, Wang DY. Interfacial engineering of layered double hydroxide toward epoxy resin with improved fire safety and mechanical property. Compos B Eng 2018;152:336–46.
[18] Du BX, Fang ZP. The preparation of layered double hydroxide wrapped carbon nanotubes and their application as a flame retardant for polypropylene. Nanotechnology 2010;21:315603.
[19] Li Z, Liu LJ, González AJ, Wang DY. Bioinspired polydopamine-induced assembly of ultrafine $Fe(OH)_3$ nanoparticles on halloysite toward highly efficient fire retardancy of epoxy resin via an action of interfacial catalysis. Polym Chem 2017;8:3926–36.
[20] Qin S, Pour MG, Lazar S, Köklükaya O, Gerringer J, Song YX, Wågberg L, Grunlan JC. Super gas barrier and fire resistance of nanoplatelet/nanofibril multilayer thin films. Adv Mater Interfaces 2018;6:1801424.
[21] Carosio F, Pierro AD, Alongi J, Fina A, Saracco G. Controlling the melt dripping of polyester fabrics by tuning the ionic strength of polyhedral oligomeric silsesquioxane and sodium montmorillonite coatings assembled through Layer by Layer. J Colloid Interface Sci 2018;510:142–51.
[22] Xue YJ, Shen MX, Zeng SH, Zhang W, Hao LY, Yang L, Song PA. A novel strategy for enhancing the flame resistance, dynamic mechanical and the thermal degradation properties of epoxy nanocomposites. Mater Res Express 2019;6:125003.
[23] Wang X, Kalali EN, Wan JT, Wang DY. Carbon-family materials for flame retardant polymeric materials. Prog Polym Sci 2017;69:22–46.
[24] Feng YZ, Han GJ, Wang B, Zhou XP, Ma JM, Ye YS, Liu CT, Xie XL. Multiple synergistic effects of graphene-based hybrid and hexagonal born nitride in enhancing thermal conductivity and flame retardancy of epoxy. Chem Eng J 2020;379:122402.
[25] Fang F, Song PA, Ran SY, Guo ZH, Wang H, Fang ZP. A facile way to prepare phosphorus-nitrogen-functionalized graphene oxide for enhancing the flame retardancy of epoxy resin. Comput Commun 2018;10:97–102.
[26] Xu ZG, Song PA, Zhang J, Guo QP, Mai YW. Epoxy nanocomposites simultaneously strengthened and toughened by hybridization with graphene oxide and block ionomer. Compos Sci Technol 2018;168:363–70.
[27] Huang GB, Chen W, Wu T, Guo HC, Fu CY, Xue YJ, Wang K, Song PA. Multifunctional graphene-based nano-additives toward high-performance polymer nanocomposites with enhanced mechanical, thermal, flame retardancy and smoke suppressive properties. Chem Eng J https://doi.org/10.1016/j.cej.2020.127590..
[28] Zhang JH, Kong QH, Wang DY. Simultaneously improving the fire safety and mechanical properties of epoxy resin with Fe-CNTs via large-scale preparation. J Mater Chem A 2018;6:6376–86.
[29] Wen X, Gong J, Yu HO, Liu Z, Wan D, Liu J, Jiang ZW, Tang T. Catalyzing carbonization of poly(L-lactide) by nanosized carbon black combined with Ni_2O_3 for improving flame retardancy. J Mater Chem 2012;22:19974–80.
[30] Wen X, Min JK, Tan HY, Gao DD, Chen XC, Szymańska K, Zielińska B, Mijowska E, Tang T. Reactive construction of catalytic carbonization system in $PP/C_{60}/Ni(OH)_2$ nanocomposites for simultaneously improving thermal stability, flame retardancy and mechanical properties. Compos Part A-Appl S 2020;129:105722.
[31] Guo ZH, Ye RF, Zhao LP, Ran SY, Fang ZP, Li J. Fabrication of fullerene-decorated graphene oxide and its influence on flame retardancy of high density polyethylene. Compos Sci Technol 2016;129:123–9.
[32] Xue YJ, Feng JB, Huo SQ, Song PA, Yu B, Liu L, Wang H. Polyphosphoramide-intercalated MXene for simultaneously enhancing thermal stability, flame retardancy and mechanical properties of polylactide. Chem Eng J 2020;397:125336.
[33] Gao YS, Wu JW, Wang Q, Wilkie CA, O'Hare D. Flame retardant polymer/layered double hydroxide nanocomposites. J Mater Chem A 2014;2:10996–1016.
[34] Zhang ZD, Qin JY, Zhang WC, Pan YT, Wang DY, Yang RJ. Synthesis of a novel dual layered double hydroxide hybrid nanomaterial and its application in epoxy nanocomposites. Chem Eng J 2020;381:122777.
[35] Sai T, Ran SY, Guo ZH, Yan HQ, Zhang Y, Wang H, Song PA, Fang ZP. Transparent, highly thermostable and flame retardant polycarbonate enabled by rod-like phosphorous-containing metal complex aggregates. Chem Eng J 2021;409:128223.
[36] Wang DS, Wen X, Chen XC, Li YH, Mijowska E, Tang T. A novel stiffener skeleton strategy in catalytic carbonization system with enhanced carbon layer structure and improved fire retardancy. Compos Sci Technol 2018;164:82–91.
[37] Zhang CG, Li JY, Shi CS, Liu EZ, Du XW, Feng W, Zhao NQ. The efficient synthesis of carbon nano-onions using chemical vapor deposition on an unsupported Ni–Fe alloy catalyst. Carbon 2011;49:1151–8.
[38] Yu ZX, Chen D, Rønning M, Vralstad T, Ochoa-Fernández E, Holmen A. Large-scale synthesis of carbon nanofibers on Ni-Fe-Al hydrotalcite derived catalysts I. Preparation and characterization of the Ni-Fe-Al hydrotalcites and their derived catalysts. Appl Catal A 2008;338:136–46.
[39] Zhang Y, Jing J, Liu T, Xi LD, Sai T, Ran SY, Fang ZP, Huo SQ, Song PA. A molecularly engineered bioderived polyphosphate for enhanced flame retardant, UV-blocking and mechanical properties of poly(lactic acid). Chem Eng J 2021;411:128493.
[40] Wang Q, Zhang X, Zhu JH, Guo ZH, O'Hare D. Preparation of stable dispersions of layered double hydroxides (LDHs) in nonpolar hydrocarbons: new routes to polyolefin/LDH nanocomposites. Chem Commun 2012;48:7450–2.
[41] Kong QH, Wu T, Tang YQ, Xiong LM, Liu H, Zhang JH, Guo RH, Zhang F. Improving thermal and flame retardant properties of epoxy resin with organic NiFe-layered double hydroxide-carbon nanotubes hybrids. Chin J Chem 2017;35:1875–80.
[42] Liu A, Tian HW, Ju XD, Wang W, Han P, Li WH. In-situ growth of layered double hydroxides nanosheet arrays on graphite fiber as highly dispersed nanofillers for polymer coating with excellent anticorrosion performances. J Taiwan Inst Chem Eng 2019;104:330–40.
[43] Sun DZ, Chu CC, Sue HJ. Simple approach for preparation of epoxy hybrid nanocomposites based on carbon nanotubes and a model clay. Chem Mater 2010;22:3773–8.
[44] Hapuarachchi TD, Peijs T. Multiwalled carbon nanotubes and sepiolite nanoclays as flame retardants for polylactide and its natural fibre reinforced composites. Compos Part A-Appl S 2010;41:954–63.
[45] Zhan ZS, Xu MJ, Li B. Synergistic effects of sepiolite on the flame retardant properties and thermal degradation behaviors of polyamide 66/aluminum diethylphosphinate composites. Polym Degrad Stabil 2015;117:66–74.
[46] Yan W, Xie P, Yang ZW, Luo GJ, Huang WJ, Tian Q, Tu CY, Zhang CM, Yang CL, Wang K. Flame-retardant behaviors of aluminum phosphates coated sepiolite in epoxy resin. J Fire Sci 2021;39(1):3–18.
[47] Zotti A, Borriello A, Ricciardi M, Antonucci V, Giordano M, Zarrelli M. Effects of sepiolite clay on degradation and fire behaviour of a bisphenol A-based epoxy. Compos B Eng 2015;73:139–48.

[48] Jiang P, Zhang S, Bourbigot S, Chen ZL, Duquesne S, Casetta M. Surface grafting of sepiolite with a phosphaphenanthrene derivative and its flame-retardant mechanism on PLA nanocomposites. Polym Degrad Stabil 2019;165:68–79.
[49] Zhang QT, Li SX, Hu XP, Wang PJ, Zeng JB, Wang XL, Wang YZ. Structure, morphology, and properties of LDPE/sepiolite nanofiber nanocomposite. Polym Adv Technol 2017;28:958–64.
[50] Han YF, Liu ZH, Yang ZP, Wang ZL, Tang XH, Wang T, Fan LH, Ooi K. Preparation of Ni^{2+}–Fe^{3+} layered double hydroxide material with high crystallinity and well-defined hexagonal shapes. Chem Mater 2008;20:360–3.
[51] Perraki T, Orfanoudaki A. Study of raw and thermally treated sepiolite from the Mantoudi area, Euboea, Greece. J Therm Anal Calorim 2008;91:589–93.
[52] Liu LB, Chen HB, Shiko E, Fan XF, Zhou YF, Zhang G, Luo X, Hua(Eric) XY. Low-cost DETA impregnation of acid-activated sepiolite for CO_2 capture. Chem Eng J 2018;353:940–8.
[53] Susanginee N, Lagnamayee M, Kulamani P. Visible light-driven novel g-C_3N_4/NiFe-LDH composite photocatalyst with enhanced photocatalytic activity towards water oxidation and reduction reaction. J Mater Chem A 2015;3:18622–35.
[54] Ghonchepour E, Islami MR, Bananezhad B, Mostafavi H, Tikdari AM. Synthesis of recoverable palladium composite as an efficient catalyst for the reduction of nitroarene compounds and Suzuki cross-coupling reactions using sepiolite clay and magnetic nanoparticles (Fe_3O_4@sepiolite-Pd^{2+}). C R Chim 2019;22:84–95.
[55] Hobbs C, Jaskaniec S, McCarthy EK, Downing C, Opelt K, Güth K, Shmeliov A, Mourad MCD, Mandel K, Nicolosi V. Structural transformation of layered double hydroxides: an in situ TEM analysis. npj 2D Mater Appl 2018;2.
[56] Tartaglione G, Tabuani D, Camino G. Thermal and morphological characterisation of organically modified sepiolite. Microporous Mesoporous Mater 2008;107:161–8.
[57] Xiao T, Tang YW, Jia ZY, Li DW, Hu XY, Li BH, Luo LJ. Self-assembled 3D flower-like Ni^{2+}-Fe^{3+} layered double hydroxides and their calcined products. Nanotechnology 2009;20:475603.
[58] Fang F, Huo SQ, Shen HF, Ran SY, Wang H, Song PA, Fang ZP. A bio-based ionic complex with different oxidation states of phosphorus for reducing flammability and smoke release of epoxy resins. Comput Commun 2020;17:104–8.
[59] Huo SQ, Liu ZT, Wang J. Thermal properties and flame retardancy of an intumescent flameretarded epoxy system containing phosphaphenanthrene, triazinetrione and piperidine. J Therm Anal Calorim 2020;139(2):1099–110.
[60] Huo SQ, Yang S, Wang J, Cheng JW, Zhang QQ, Hu YF, Ding GP, Zhang QX, Song PA. A liquid phosphorus-containing imidazole derivative as flame-retardant curing agent for epoxy resin with enhanced thermal latency, mechanical, and flame-retardant performances. J Hazard Mater 2020;386:121984.
[61] Tartaglione G, Tabuani D, Camino G, Moisio M. PP and PBT composites filled with sepiolite: morphology and thermal behaviour. Compos Sci Technol 2008;68:451–60.
[62] Wei J, Yao RW, Ge QJ, Xu DY, Fang CY, Zhang JX, Xu HY, Sun J. Precisely regulating Brønsted acid sites to promote the synthesis of light aromatics via CO_2 hydrogenation. Appl Catal, B 2021;283:119648.
[63] Jiang SD, Bai ZM, Tang G, Song L, Stec AA, Hull TR, Hu Y, Hu WZ. Synthesis of mesoporous silica@Co–Al layered double hydroxide spheres: layer-by-layer method and their effects on the flame retardancy of epoxy resins. ACS Appl Mater Interfaces 2014;6:14076–86.
[64] Wang PJ, Hu XP, Liao DJ, Wen Y, Hull TR, Miao F, Zhang QT. Dual fire retardant action: the combined gas and condensed phase effects of Azo-modified NiZnAl layered double hydroxide on intumescent polypropylene. Ind Eng Chem Res 2017;56:920–32.
[65] He WT, Song PA, Yu B, Fang ZP, Wang H. Flame retardant polymeric nanocomposites through the combination of nanomaterials and conventional flame retardants. Prog Mater Sci 2020;114:100687.
[66] Liao DJ, Xu QK, McCabe RW, Babu HV, Hu XP, Pan N, Wang DY, Hull TR. Ferrocene-based non-phosphorus copolymer: synthesis, highcharring mechanism and its application in fire retardant epoxy resin. Ind Eng Chem Res 2017;56(44):12630–43.
[67] Li P, Wang B, Liu YY, Xu YJ, Jiang ZM, Dong CH, Zhang L, Liu Y, Zhu P. Fully bio-based coating from chitosan and phytate for fire safety and antibacterial cotton fabrics. Carbohydr Polym 2020;237:116173.
[68] Qu LJ, Sui YL, Zhang CL, Li PH, Dai XY, Xu BS, Fang DN. POSS-functionalized graphene oxide hybrids with improved dispersive and smoke-suppressive properties for epoxy flame-retardant application. Eur Polym J 2020;122:109383.
[69] Pappalardo S, Russo P, Acierno D, Rabe S, Schartel B. The synergistic effect of organically modified sepiolite in intumescent flame retardant polypropylene. Eur Polym J 2016;76:196–207.
[70] Huang YB, Jiang SH, Liang RC, Sun P, Hai Y, Zhang L. Thermal-triggered insulating fireproof layers: a novel fire-extinguishing MXene composites coating. Chem Eng J 2020;391:123621.
[71] Stec AA, Hull TR, Purser JA, Purser DA. Comparison of toxic product yields from bench-scale to ISO room. Fire Saf J 2009;44:62–70.
[72] Cheng Z, Liao DJ, Hu XP, Li WX, Xie CQ, Zhang HJ, Yang WX. Synergistic fire retardant effect between expandable graphite and ferrocene-based non-phosphorus polymer on polypropylene. Polym Degrad Stabil 2020;178:109201.
[73] Wang YL, Li ZP, Li YY, Wang JY, Liu X, Song TY, Yang XM, Hao JW. Spray drying assisted Layer-by-Layer assembly of alginate, 3- aminopropyltriethoxysilane, and magnesium hydroxide flame retardant and its catalytic graphitization in ethylene-vinyl acetate resin. ACS Appl Mater Interfaces 2018;10:10490–500.
[74] Gao YB, Zhao ZZ, Jia HM, Yang XT, Lei XD, Kong XG, Zhang FZ. Partially reduced Ni^{2+}, Fe^{3+}-layered double hydroxide for ethanol electrocatalysis. J Mater Sci 2019;54:14515–23.
[75] Hong J, Wu T, Wu H, Zeng B, Zeng S, Chen T, Wang X, Lu Z, Yuan C, Balaji K, Petri DFS, Dai LZ. Nanohybrid silver nanoparticles@halloysite nanotubes coated with polyphosphazene for effectively enhancing the fire safety of epoxy resin. Chem Eng J 2021;407:127087.
[76] Li Z, Lira SIM, Zhang L, Exposito DF, Heeralal VB, Wang DY. Bio-inspired engineering of boron nitride with iron-derived nanocatalyst toward enhanced fire retardancy of epoxy resin. Polym Degrad Stabil 2018;157:119–30.
[77] Liu XF, Liu BW, Luo X, Guo DM, Zhong HY, Chen L, Wang YZ. A novel phosphorus-containing semi-aromatic polyester toward flame retardancy and enhanced mechanical properties of epoxy resin. Chem Eng J 2020;380:122471.
[78] Zhu MH, Liu L, Wang ZZ. Mesoporous silica via self-assembly of nano zinc amino-tris-(methylenephosphonate) exhibiting reduced fire hazards and improved impact toughness in epoxy resin. J Hazard Mater 2020;392:122343.
[79] Huo SQ, Yang S, Wang J, Cheng JW, Zhang QQ, Hu YF, Ding GP, Zhang QX, Song PA, Wang H. A liquid phosphaphenanthrene-derived imidazole for improved flame retardancy and smoke suppression of epoxy resin. ACS Appl Polym Mater 2020;2(8):3566–75.
[80] Karami Z, Jouyandeh M, Ali JA, Ganjali MR, Aghazadeh M, Paran SMR, Naderi G, Puglia D, Saeb MR. Epoxy/layered double hydroxide (LDH) nanocomposites: synthesis, characterization, and Excellent cure feature of nitrate anion intercalated Zn-Al LDH. Prog Org Coating 2019;136:105218.
[81] Fang F, Ran SY, Fang ZP, Song PA, Wang H. Improved flame resistance and thermo-mechanical properties of epoxy resin nanocomposites from functionalized graphene oxide via self-assembly in water. Compos B Eng 2019;165:406–16.
[82] Zhang J, Li Z, Shao ZB, Zhang L, Wang DY. Hierarchically tailored hybrids via interfacial-engineering of self-assembled UiO-66 and prussian blue analogue: novel strategy to impart epoxy high efficient fire retardancy and smoke suppression. Chem Eng J 2020;400:125942.